Reconstruction of phase maps from the configuration of phase singularities in two-dimensional manifolds

Antoine Herlin and Vincent Jacquemet

Institut de Génie Biomédical, Department of Physiology,

Faculty of Medicine, Université de Montréal, Montréal, Canada;

Centre de Recherche, Hôpital du Sacré-Coeur de Montréal.

Abstract

Phase singularity analysis provides a quantitative description of spiral wave patterns observed in chemical or biological excitable media. The configuration of phase singularities (locations and directions of rotation) is easily derived from phase maps in two-dimensional manifolds. The question arises whether one can construct a phase map with a given configuration of phase singularities. The existence of such phase map is guaranteed provided that the phase singularity configuration satisfies a certain constraint associated with the topology of the supporting medium. This paper presents a constructive mathematical approach to numerically solve this problem in the plane, on the sphere as well as in more general geometries relevant to atrial anatomy including holes and a septal wall. This tool can notably be used to create initial conditions with controllable spiral wave configuration for cardiac propagation models and thus help in the design of computer experiments in atrial electrophysiology.

I. INTRODUCTION

Formation of complex patterns such as multiple spiral waves has been observed in chemical and biological excitable media [1]. These phenomena can be reproduced in mathematical models governed by a reaction-diffusion system [2]. When local excitation is cyclic (though not necessarily periodic), a phase (between 0 and 2π, modulo 2π) can be defined to represent the position within the cycle [3, 4]. A phase map describes the state of the system over space at a given instant in time. There may be points called phase singularities at which the phase cannot be well-defined (the phase map is discontinuous at these points). In two-dimensional systems, phase singularities are located near the tip of spiral waves. Phase singularity identification and tracking provide a tool for characterizing the spatio-temporal complexity of the dynamics in excitable media [4]. Applications include cardiac propagation models in which the presence of spiral waves is associated with arrhythmia.

The topology of the medium constrains the type of wave patterns that can be observed [1, 3]. In the atria, the anatomical substrate consists in a thin-walled three-dimensional medium (that can be considered two-dimensional in first approximation) with holes corresponding to the insertion of veins and valves, thus creating a complicated topological space. Necessary conditions for the existence of a spiral wave pattern with given distribution of phase singularities have been identified [5–7]. These constraints depend on the topology of the

medium. A more difficult problem is to find sufficient conditions for the existence of a spiral wave pattern (is it possible to connect phase singularities with wave fronts and reconstruct a phase map?). Cruz-White demonstrated that the necessary conditions were indeed sufficient. Her theoretical arguments, however, gave little information about how to practically perform the task of phase map reconstruction.

In this paper, the problem of exhibiting a phase map with given configuration of phase singularities (locations and directions of rotation) is considered. An algorithm is developed to numerically solve this problem in different two-dimensional geometries/topologies relevant to heart anatomy. A dedicated phase map filtering method is used to highlight the structure of the spiral wave pattern. The approach is illustrated in two different surface models of the human atria. This computational framework forms a sound mathematical basis to create initial conditions for reaction-diffusion systems, while eliminating the limitations of previous approaches [8, 9].

II.   PROBLEM STATEMENT

A phase field $\theta(\mathbf{x})$ in a two-dimensional orientable connected manifold S (including h holes with boundaries $H_1, \ldots, H_h$) is defined here as a real function with values modulo 2π that is smooth everywhere in S except at a finite number (n) of points $\mathbf{x}_1, \ldots, \mathbf{x}_n$. The topological charge q_k of the discontinuity $\mathbf{x}_k$ is defined as the contour integral [5]

$$q_k = \frac{1}{2\pi} \oint_{\Gamma_k} \nabla\theta \cdot \mathrm{d}\boldsymbol{\ell} \ , \tag{1}$$

where Γ_k is a closed curve encircling the point $\mathbf{x}_k$ but none of the other discontinuity points and none of the holes. The orientation of the curve Γ_k follows the orientation of the surface S. The value of q_k is an integer that does not depend on the curve Γ_k as long as Γ_k satisfies these constraints. When q_k is nonzero, $\mathbf{x}_k$ is called a phase singularity. Similarly, the topological charge of the hole H_k, denoted by Q_k, is defined as the integral (1) over the closed contour H_k. Notations are illustrated in Fig. 1.

From a given phase field θ, the list of phase singularities and their topological charge can be determined [4]. Two questions arise: (1) whether there exists a phase field with a given configuration of phase singularities $\{(\mathbf{x}_k, q_k), k = 1 \ldots n\}$ and topological charges of holes $\{(H_k, Q_k), k = 1 \ldots h\}$, and (2) how to construct one. Conditions for the existence of

a solution are given in Sect. III. An algorithm to construct such a solution is developed in Sect. IV.

III.   EXISTENCE OF A SOLUTION

Using topological arguments based on homotopy and homology theories, Cruz-White demonstrated the following theorem [6]: if S is a two-dimensional orientable compact connected manifold with h holes, there exists a phase field θ with n phase singularities at $\mathbf{x}_k$ with topological charges q_k, $k = 1 \ldots n$, and with topological charge Q_k at hole k, $k = 1 \ldots h$, *if and only if* the constraint

$$\sum_{k=1}^{n} q_k = \sum_{k=1}^{h} Q_k \tag{2}$$

is satisfied. Proof is given in [6].

Clearly, if θ is a solution, $\theta + \chi \mod 2\pi$ is also a solution if χ is smooth everywhere in S, including all the $\mathbf{x}_k$. Consequently, there is either no solution or an infinite number of solutions.

IV.   CONSTRUCTION OF A SOLUTION

The existence of a solution depends on the topology of the domain S. In this section, a solution is constructed for different geometries of increasing complexity.

A.   Solution in the plane

In the plane (unbounded, no hole, see Fig. 1A), a point $\mathbf{x}$ can be represented by a complex number $z(\mathbf{x})$, and the locations $\mathbf{x}_k$ of the phase singularities by $z_k = z(\mathbf{x}_k)$. The function

$$\theta_{\text{plane}}(z) = \arg \prod_{m=1}^{n} (z - z_m)^{q_m} \tag{3}$$

is a solution to the problem ('arg' denotes the argument/phase of a complex number). The only singularities are found at $z = z_k$, $k = 1 \ldots n$, where the product vanishes. If Γ_k is a

4

circle of (small enough) radius r centered at $\mathbf{x}_k$, the topological charge q around $\mathbf{x}_k$ reads:

$$q = \frac{1}{2\pi} \oint_{\Gamma_k} \nabla\theta_{\text{plane}} \cdot \mathrm{d}\boldsymbol{\ell} \tag{4}$$

$$= \frac{1}{2\pi} \oint_{\Gamma_k} \nabla \arg (z - z_k)^{q_k} \cdot \mathrm{d}\boldsymbol{\ell} + \sum_{m \neq k} \frac{1}{2\pi} \oint_{\Gamma_k} \nabla \arg (z - z_m)^{q_m} \cdot \mathrm{d}\boldsymbol{\ell} . \tag{5}$$

The second term is zero since the argument of $(z - z_m)^{q_m}$ is smooth in the vicinity of $\mathbf{x}_k$. If Γ_k is parametrized by $z(t) = z_k + re^{it}$ for $t \in [0, 2\pi]$ and r small enough, the topological charge q is expressed as

$$q = \frac{1}{2\pi} \int_0^{2\pi} \frac{\mathrm{d}}{\mathrm{d}t} \left(\arg e^{iq_k t} \right) \mathrm{d}t = q_k , \tag{6}$$

which demonstrates that θ has a phase singularity at $\mathbf{x}_k$ with topological charge q_k. There is no constraint on the sum of topological charges. This is not a contradiction with the theorem of Sect. III since the domain is not compact.

B. Solution in a planar domain with holes

If an infinite planar domain S has holes (see Fig. 1B), new points $\mathbf{x}_{n+1}, \ldots, \mathbf{x}_{n+h}$ are defined such that $\mathbf{x}_{n+k}$ is located inside the hole H_k (outside S, see Fig. 1). The orientation of the closed curves H_k (boundary of S) derives from the orientation of the surface in such a way that the Stokes' theorem may naturally be applied. The orientation of Γ_{n+k} $(k = 1 \ldots h)$ is, however, kept the same as that of Γ_k $(k = 1 \ldots n)$ so that the singularities may be referred to as clockwise or counterclockwise. The method of Subsect. IV A is then applied to the phase singularity configuration $\{(\mathbf{x}_k, q_k), k = 1 \ldots n\} \cup \{(\mathbf{x}_{n+k}, -Q_k), k = 1 \ldots h\}$. The restriction of θ_{plane} to S provides the desired solution. Since $\mathbf{x}_{n+k}$ is placed outside S, only n phase singularities are created. Moreover, the hole k holds a topological charge of

$$\frac{1}{2\pi} \oint_{H_k} \nabla\theta_{\text{plane}} \cdot \mathrm{d}\boldsymbol{\ell} = -\frac{1}{2\pi} \oint_{\Gamma_{n+k}} \nabla\theta_{\text{plane}} \cdot \mathrm{d}\boldsymbol{\ell} = Q_k , \tag{7}$$

as expected (see Fig. 1B). There is again no constraint on q_k and Q_k.

If the planar domain is bounded (and thus compact; see Fig. 1C), the outer boundary is assumed to be H_h. The same method is applied to the phase singularity configuration $\{(\mathbf{x}_k, q_k), k = 1 \ldots n\} \cup \{(\mathbf{x}_{n+k}, -Q_k), k = 1 \ldots h - 1\}$, i.e., the outer boundary is ignored.

The topological charge of the boundary H_h is

$$\frac{1}{2\pi} \oint_{H_h} \nabla\theta_{\mathrm{plane}} \cdot \mathrm{d}\boldsymbol{\ell} = -\sum_{k=1}^{h-1} \frac{1}{2\pi} \oint_{H_k} \nabla\theta_{\mathrm{plane}} \cdot \mathrm{d}\boldsymbol{\ell} + \sum_{k=1}^{n} \frac{1}{2\pi} \oint_{\Gamma_k} \nabla\theta_{\mathrm{plane}} \cdot \mathrm{d}\boldsymbol{\ell} \tag{8}$$

$$= -\sum_{k=1}^{h-1} Q_k + \sum_{k=1}^{n} q_k \; , \tag{9}$$

which is equal to Q_h if and only if the constraint (2) is satisfied. If Q_h is not specified and can take any value, there is always a solution.

C. Solution on the sphere

The solution on the unit sphere ($\|\mathbf{x}\| = 1$) can be expressed in terms of the solution in a plane through the stereographic transformation. The north pole is placed on a phase singularity, for instance $\mathbf{x}_n$. Unit vectors $\mathbf{u}$ and $\mathbf{v}$ are chosen such that $(\mathbf{u}, \mathbf{v}, \mathbf{x}_n)$ forms a positively-oriented orthonormal basis. Using the stereographic mapping

$$z_{\mathrm{stereo}}(\mathbf{x}) = \frac{(\mathbf{u} + i\,\mathbf{v}) \cdot \mathbf{x}}{1 - \mathbf{x}_n \cdot \mathbf{x}} \; , \tag{10}$$

the phase singularities $\mathbf{x}_1 \ldots \mathbf{x}_{n-1}$ are projected on the complex plane and $\mathbf{x}_n$ is sent to infinity. Because this mapping is a diffeomorphism, it preserves phase singularities and topological charges. The phase field on the sphere is given by

$$\theta_{\mathrm{sphere}}(\mathbf{x}) = \theta_{\mathrm{plane}}(z_{\mathrm{stereo}}(\mathbf{x})) \tag{11}$$

where θ_{plane} is computed in an infinite planar domain using Eq. (3) with $n - 1$ phase singularities at $z_k = z_{\mathrm{stereo}}(\mathbf{x}_k)$ for $k = 1 \ldots n - 1$. The value of $\theta_{\mathrm{sphere}}(\mathbf{x}_n)$ is not defined and can be assigned any value since θ_{sphere} is by construction discontinuous at $\mathbf{x}_n$. By the same argument as in Subsect. IV B, $q_n = -\sum_{k=1}^{n-1} q_k$, *i.e.*, the sum of all topological charges must be zero [5].

If the sphere includes holes, the north pole can be placed in one of the holes. In this case, the stereographic transformation maps the punctured sphere onto a planar bounded domain with holes. The formula (11) combined with the method from Subsect. IV B therefore provides the solution. As a result, the constraint (2) also applies.

6

D. Solution in a manifold with spherical topology

If the manifold S is homeomorphic to a sphere, there exists a continuous invertible mapping $F(\mathbf{x})$ from S to the unit sphere (invertible implies that there is no folding), so that the phase field $\theta_S(\mathbf{x})$ on S can be written as

$$\theta_S(\mathbf{x}) = \theta_{\text{sphere}}(F(\mathbf{x})) \tag{12}$$

where θ_{sphere} is computed using n phase singularities at $F(\mathbf{x}_k)$ for $k = 1 \dots n$. If S is described by a triangulated surface, specific algorithms have been developed to numerically construct a mapping F that projects the surface onto the unit sphere [10], which makes Eq. (12) relevant for practical applications.

If holes are present, they are filled first by adding a node at the center of gravity of the hole and by creating the triangles that connect that new node to the boundary of the hole. Provided that this new closed surface is homeomorphic to a sphere, F is computed for this new surface, formula (12) is applied, and the new node and triangles are discarded.

E. Extension to non-manifold topology

Non-manifold topology notably arises when two surfaces intersect along a curve. As an example relevant to atrial anatomy, consider a surface S_1 with spherical topology (right and left atrial epicardium) and a surface S_2 with the topology of a disc (septum) such that their intersection is a closed curve Γ ($S = S_1 \cup S_2$, $\Gamma = S_1 \cap S_2$), as illustrated in Fig. 2. If there are holes, these holes can be filled as in the previous subsection. Γ divides S_1 into two manifolds S_1^r (right) and S_1^l (left). Orientation of S_2 is chosen such that $S_2 \cup S_1^r$, which also has spherical topology, is consistently oriented. The problem is to find a phase field θ defined on S with phase singularities at $\mathbf{x}_{1,k}$ with topological charge $q_{1,k}$, $k = 1 \dots n_1$, in S_1 and at $\mathbf{x}_{2,k}$ with topological charge $q_{2,k}$, $k = 1 \dots n_2$, in S_2. In S_1, this list consists of phase singularities in the right part ($q_{1,k}^r$ at $\mathbf{x}_{1,k}^r$, $k = 1 \dots n_1^r$) and in the left part ($q_{1,k}^l$ at $\mathbf{x}_{1,k}^l$, $k = 1 \dots n_1^l$) where of course $n_1 = n_1^r + n_1^l$.

A phase field θ_1 is first constructed in S_1 using the method of Subsect. IV D. This assumes $\sum_{k=1}^{n_1} q_{1,k} = 0$. A phase field θ_2 is obtained the same way in S_2 or using the method of Subsect. IV B if S_2 can be conveniently projected on a plane. Then, θ is set to θ_1 in S_1 and $\theta_2 + \chi$ (mod 2π) in S_2, where $\chi(\mathbf{x})$ is a correction field applied to θ_2 to ensure the continuity

of θ on Γ. To determine χ, the value of χ on the boundary Γ is set to the phase-unwrapped version of $\theta_1 - \theta_2$ (not necessarily restricted to the interval from 0 to 2π). Its value inside S_2 is obtained by Laplacian interpolation ($\Delta\chi = 0$ in S_2). If the condition $\oint_\Gamma \nabla\theta_1 \cdot \mathrm{d}\boldsymbol{\ell} = \oint_\Gamma \nabla\theta_2 \cdot \mathrm{d}\boldsymbol{\ell}$ is verified, χ has no 2π-jump on Γ and is therefore also continuous in S_2. In this case, the number and location of phase singularities are preserved by the correction χ. This constraint can be written as

$$\sum_{k=1}^{n_1^r} q_{1,k}^r = -\sum_{k=1}^{n_1^l} q_{1,k}^l = -\sum_{k=1}^{n_2} q_{2,k} \tag{13}$$

which indicates that the sum of topological charges must be zero both in S_1 and $S_1^r \cup S_2$.

V. PHASE MAP POSTPROCESSING

Once a solution θ is found, any phase field of the form $\theta + \chi \mod 2\pi$ provides another solution if χ is smooth everywhere. The function χ will be chosen so as to reduce the distortions caused by the different transformations (e.g. from the plane to the sphere and from the sphere to an arbitrary surface) and to highlight the presence and the direction of rotation of phase singularities, based on methods presented in [11].

The complex phase field ϕ is defined as $\exp(i\theta)$. This field is iteratively transformed through the mapping $\phi \mapsto \phi \exp(i\chi)$, where χ is the solution to an equation $\mathcal{F}[\chi, \phi] = 0$. The postprocessing procedure is performed in two steps, each one using a specific operator $\mathcal{F}$.

A. Phase map smoothing

To regularize the phase map, the idea is to force the Laplacian to be zero in the domain, i.e., $\Delta(\theta + \chi) = 0$. To evaluate $\Delta\theta$ without numerical issues related to 2π-jumps, the relation $\Delta\theta = \mathrm{Im}\, \nabla \cdot (\phi^* \nabla \phi)$ is used ('Im' is the imaginary part and the star (*) is the complex conjugate), leading to the following definition for $\mathcal{F}$:

$$\mathcal{F}[\chi, \phi] = \Delta\chi + \mathrm{Im}\, \nabla \cdot (\phi^* \nabla \phi) \, . \tag{14}$$

No-flux boundary condition is used, except on the small circuits Γ_k around the phase singularities, where χ is set to zero. This equation is solved for χ using dedicated finite element methods on a triangulated mesh [11].

B. Enhancement of spiral-like patterns

To reconstruct spiral-like patterns rotating around each phase singularity in the direction associated with the topological charge, the eikonal-diffusion equation is iteratively solved, as proposed in [9]. This equation reads $c\|\nabla\theta\| = 1 + D\Delta\theta$, where c is the normalized wavefront propagation velocity and D is a diffusion coefficient [8, 12], and establishes that wavefront propagation velocity is essentially uniform. As demonstrated in [8], the generalized Newton zero-finding method applied to this nonlinear equation consists in solving $\mathcal{F}[\chi, \phi] = 0$ where $\mathcal{F}$ is defined as:

$$\mathcal{F}[\chi, \phi] = c \, \frac{\mathrm{Im} \, \phi \, \nabla\phi^*}{\|\nabla\phi\|} \, \nabla\chi + D\Delta\chi + 1 - c \, \|\nabla\phi\| + D \, \mathrm{Im} \, \nabla \cdot (\phi^*\nabla\phi) \, . \qquad (15)$$

Again, no-flux boundary condition is used, except on the small circuits Γ_k around the phase singularities, where χ is set to zero. Dedicated finite element methods for this equation can be found in [11]. Iterations are run until wavefront velocity $\|\nabla\phi\|^{-1}$ is sufficiently uniform [9].

VI. RESULTS

A. Phase map generation in a surface with holes

The phase map generation procedure is illustrated here in a triangular mesh (about 5,000 nodes) representing the atrial epicardium derived from magnetic resonance images of a patient (Fig. 3C). Three phase singularities are introduced: one clockwise ($q_1 = -1$) and one counterclockwise ($q_2 = +1$) in the left atrium near the pulmonary veins, and one clockwise ($q_3 = -1$) in the right atrium. The tricuspid valve (TV) has a topological charge of $Q_1 = -1$ (counterclockwise rotation), while the other holes have a topological charge of zero. The relation $q_1 + q_2 + q_3 = Q_1$ is satisfied; therefore a solution exists. The atrial geometry (Fig. 3C) is mapped onto a sphere (without folding) using the Control of Area and Length Distortion (CALD) algorithm [10] implemented in the SPHARM-MAT Matlab toolbox (Li Shen, Indiana University School of Medicine). The resulting spherical geometry is shown in Fig. 3B. The sphere is projected on the plane using the stereographic projection (Eq. (10)), the north pole being placed at the center of gravity of the tricuspid valve (Fig. 3A). Lines of constant phase will be called isochrones because of their interpretation in the context of wavefront propagation [9].

9

The phase map is first computed in the plane (Eq. (3); Fig. 3A), then projected on the sphere (Eq. (11); Fig. 3B), and finally mapped onto the atrial surface (Eq. (12); Fig. 3C). Although isochrones are smooth in the plane and on the sphere (an analytical formula for the phase is used), the nonlinear transform mapping the atrial surface onto the sphere introduces severe distortions. The application of the smoothing filter (Subsect. V A) clearly regularizes the isochrones (Fig. 3D). Since the direction of rotation is not obvious in Fig. 3D, the eikonal-based filter (Subsect. V B) is applied to enhance spiral-like patterns and make the distance between isochrones more uniform (Fig. 3E).

B.   Phase map generation in a nonmanifold geometry

The case of nonmanifold geometry (Subsect. IV E) is illustrated in another triangular mesh of the atria including a septal wall. The surface S_1 is the left and right epicardium and the surface S_2 is the septum (Fig. 4A). Three phase singularities are introduced: one counterclockwise in the right atrium ($n_1^r = 1$, $q_{1,1}^r = +1$), one clockwise in the left atrium ($n_1^l = 1$, $q_{1,1}^l = -1$) and one clockwise in the septum ($n_2 = 1$, $q_{2,1} = -1$). Note that, by convention, the orientation of the septum is the same as that of the right atrium, so when seen from the right (as in Fig. 4) the orientation of the septum appears inverted. The necessary and sufficient conditions for the existence of the solution (Eq. (13)) are both verified: $q_{1,1}^r + q_{1,1}^l = 0$ and $q_{1,1}^r + q_{2,1} = 0$.

The phase map is first computed independently in the epicardium and in the septum (Fig. 4A) using the same steps as in the previous subsection. A correction field is then applied to the septum to ensure the continuity of the solution (Fig. 4B). The final solution after filtering is displayed in Fig. 4C.

VII.   DISCUSSION AND CONCLUSION

This paper provides a mathematical and computational framework for the construction of phase maps with given number and location of phase singularities, as long as the topological constraint (2) is satisfied. A first application of this tool is the initiation of spiral wave dynamics with controllable degree of complexity in a reaction-diffusion system, for instance a cardiac propagation model [9]. In this case, the phase map is used to construct an initial

condition for the partial differential equation governing wave propagation. The proposed formulas are notably applicable to atrial geometries incorporating major anatomical features, as demonstrated in the examples of Sect. VI. Combined with a random distribution of phase singularities [9], many independent realizations of the same dynamics can be easily simulated, which opens the way to statistical analysis of the evolution. The two-dimensional nature of the method, however, limits its use to thin-walled geometries (such as the atria). Although an extension to three dimensions of the theorem of Sect. III has been proved [6], its numerical implementation remains challenging.

Another application is Laplacian interpolation of angular data on a surface [13] based on its values on the boundaries (holes), *i.e.*, solving $\Delta\theta = 0$ in S with $\theta = \theta_0$ on the boundary ∂S where θ and θ_0 are defined modulo 2π. From the topological charges of the holes computed from θ_0, a phase field $\tilde{\theta}$ compatible with these topological constraints is created in S. The existence of a continuous solution depends again on the constraint (2). Then, the problem $\Delta(\theta - \tilde{\theta}) = 0$ in S with $\theta = \theta_0 - \tilde{\theta}$ on ∂S can be solved using standard methods since $\theta_0 - \tilde{\theta}$ has no phase singularity and no 2π-jump. This is essentially what was done in Subsect. V A.

Since the methods presented here explicitly take advantage of the topology of the domain, they are not applicable in the case of an arbitrary topology. A major computational problem remains the construction of a diffeomorphism to transform an arbitrary geometry into a reference geometry with the same topology (*e.g.*, a torus), for which the problem can be solved. If phase singularities are allowed to be created in addition to the desired ones, however, a simple solution can be obtained by Laplacian interpolation of the complex phase field $\phi = \exp(i\theta)$ as proposed in [9]. In this case, the constraint (2) does not have to be verified; additional phase singularities will be automatically created to satisfy the appropriate topological constraints.

The proposed method is both computationally efficient and easy to implement. It provides a solution to a sufficiently wide range of topologies to be used in practical applications, notably in atrial electrophysiology simulations. With the help of this new tool, the concept of phase singularity becomes not only useful for data analysis, but also as a way to design *in silico* experiments.

ACKNOWLEDGMENTS

[1] A. T. Winfree, *The Geometry of Biological Time* (Springer-Verlag, New York, 2001).

[2] J. P. Keener and J. Sneyd, *Mathematical Physiology*, 2nd ed., Interdisciplinary applied mathematics ; v. 8 (Springer, New York, 2001).

[3] A. T. Winfree and S. H. Strogatz, Physica D, **8**, 35 (1983).

[4] A. N. Iyer and R. A. Gray, Ann Biomed Eng, **29**, 47 (2001).

[5] J. Davidsen, L. Glass, and R. Kapral, Phys Rev E, **70**, 056203 (2004).

[6] I. Cruz-White, *Topology of spiral waves in excitable media*, Ph.D. thesis, Florida State University (2003).

[7] D. Sumners, in *Graph Theory and Topology in Chemistry* (Elsevier, Netherlands, 1987) p. 3.

[8] V. Jacquemet, IEEE Trans Biomed Eng, **57**, 2090 (2010).

[9] A. Herlin and V. Jacquemet, Chaos, **21**, 043136 (2011).

[10] L. Shen and F. Makedon, Image Vision Comput, **24**, 743 (2006).

[11] V. Jacquemet, Comput Methods Programs Biomed, **DOI: 10.1016/j.cmpb.2011.05.003** (2011).

[12] K. A. Tomlinson, P. J. Hunter, and A. J. Pullan, SIAM J Appl Math, **63**, 324 (2002).

[13] A. Chessel, F. Cao, and R. Fablet, in *Proc. European Conf. Comp. Vision (ECCV'06)*, Vol. 3951 (LNCS) (Graz, Austria, 2006) pp. 241–254.
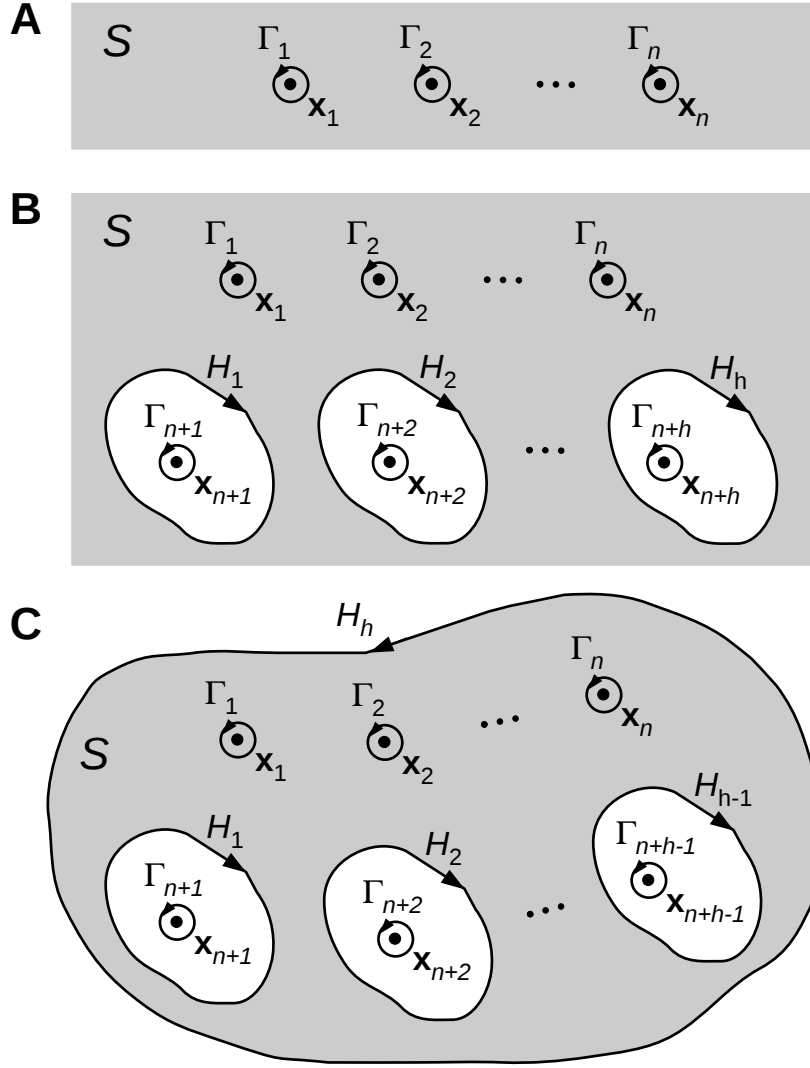
FIG. 1. Notations for (A) an unbounded planar domain, (B) an unbounded planar domain with holes, and (C) a bounded planar domain with holes. In the domain S, n phase singularities are located at $\mathbf{x}_1, \ldots, \mathbf{x}_n$ and encircled by closed contours $\Gamma_1, \ldots, \Gamma_n$; h holes/boundaries $H_1, \ldots, H_h$ are present, the last one being the exterior boundary (if any); arrows show the orientation of the contours Γ_k and H_k; inside each hole H_k, a "virtual" phase singularity is placed at $\mathbf{x}_{n+k}$ and is encircled by the closed contour Γ_{n+k}.
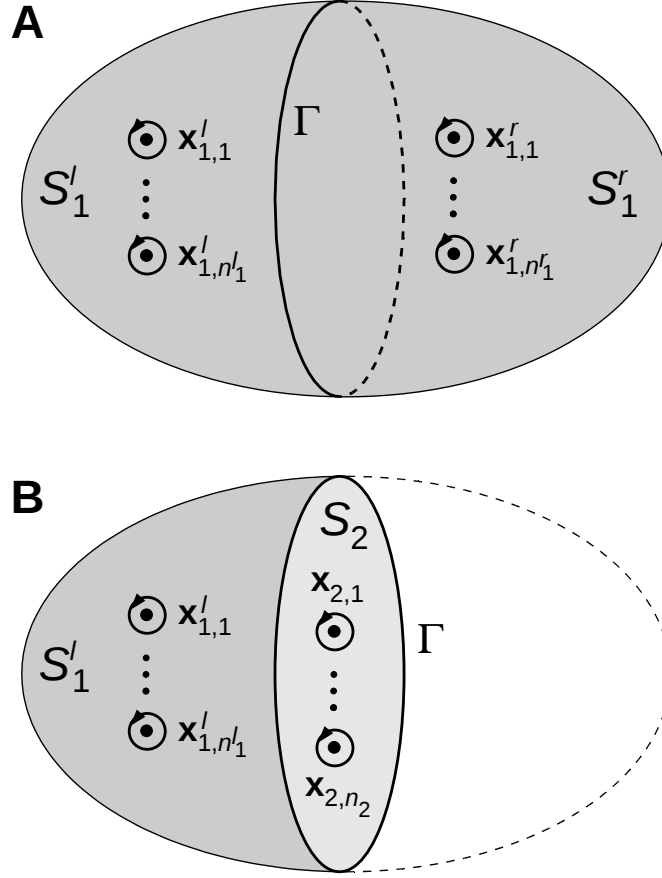
FIG. 2. Notations for a nonmanifold geometry schematically representing the atria. (A) outer surface S_1 with spherical topology composed of a right part S_1^r and a left part S_1^l separated by the curve Γ; (B) the right part is removed to make the S_2 surface ("septum") visible. In the outer surface S_1, n_1^r phase singularities are placed in the right part and n_1^l on the left part. The surface S_2 contains n_2 phase singularities. The curve Γ makes the connection between S_1 and S_2.
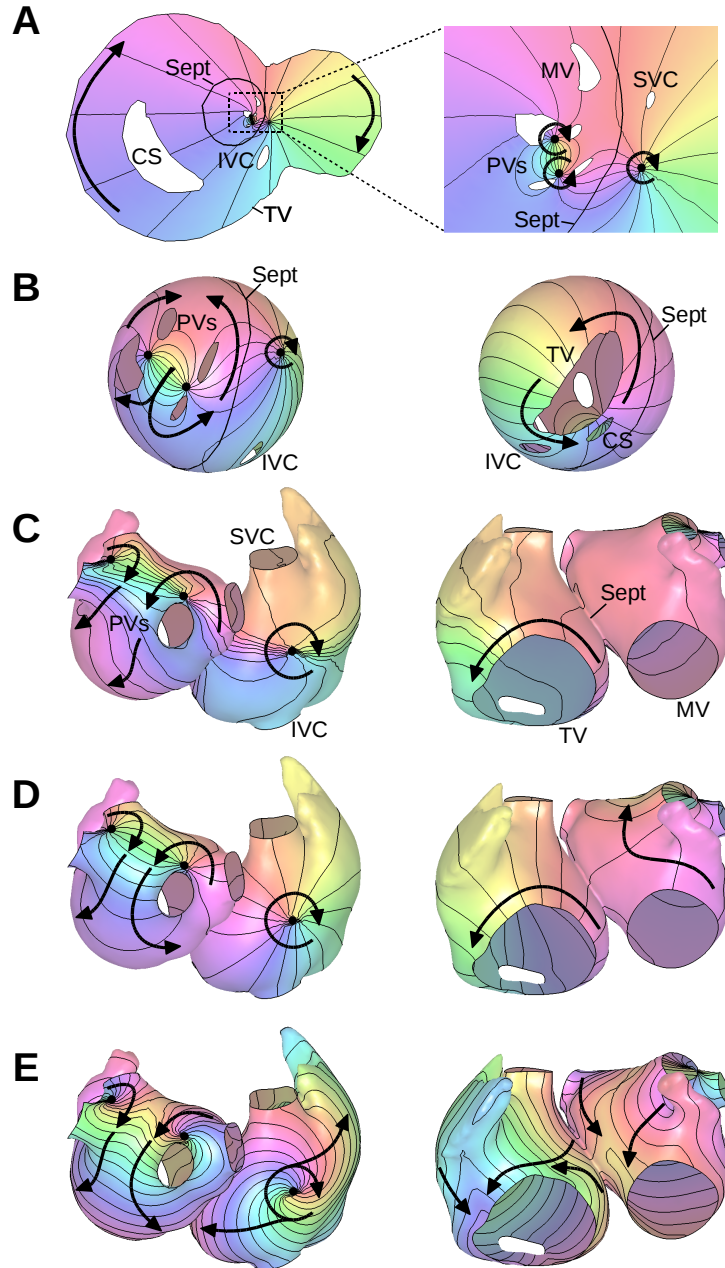
FIG. 3. (Color online) Successive steps for the generation of a phase map with 3 phase singularities in a surface model of the atria. (A) phase map computed on the plane; a zoom of the central rectangular region is displayed on the right; (B) the same phase map projected on the sphere using the inverse stereographic projection; (C) the same phase map projected on the atrial surface (posterior view on the left, anterior view on the right); (D) phase map after smoothing; (E) phase map after spiral-like pattern enhancement. Phase is color coded (graylevel coded); 16 isochrones are shown as black solid lines. Arrows represents direction of propagation (phase gradient). TV: tricuspid valve; MV: mitral valve; PVs: pulmonary veins; IVC: inferior vena cava; SVC: superior vena cava; CS: coronary sinus; Sept: septum.
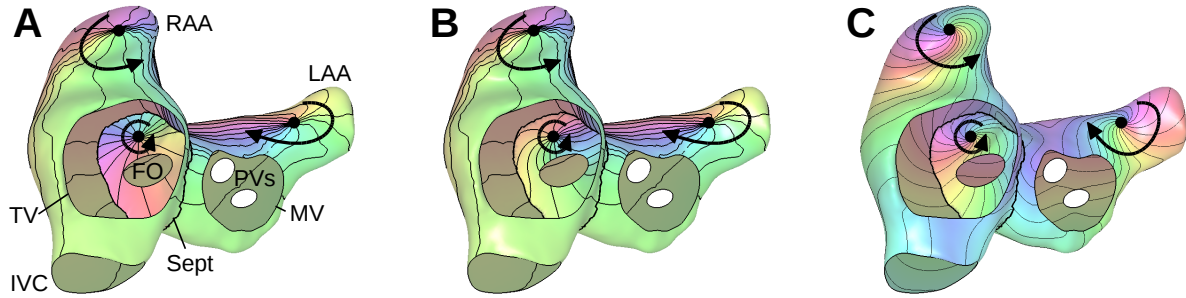
FIG. 4. (Color online) Generation of a phase map in a nonmanifold with 3 phase singularities in a surface model of the atria including a septal wall (front view). (A) Phase map constructed independently in the epicardium and in the septum; (B) phase map after correction for continuity; (C) phase map after smoothing and spiral-like pattern enhancement. Phase is color coded (graylevel coded); 16 isochrones are shown as black solid lines. Arrows represents direction of propagation (phase gradient). RAA: right atrium appendage; LAA: left atrium appendage; TV: tricuspid valve; MV: mitral valve; IVC: inferior vena cava; PVs: pulmonary veins; Sept: septum; FO: fossa ovalis.